ACS Photonics

Article

pubs.acs.org/journal/apchd5

Unidirectional Lasing Emissions from $CH_3NH_3PbBr_3$ Perovskite Microdisks

Kaiyang Wang,[†,‡] Wenzhao Sun,[†,‡] Jiankai Li,[†] Zhiyuan Gu,[†] Shumin Xiao,[§] and Qinghai Song*[,†]

[†]National Key Laboratory of Tunable Laser Technonlogy, Integrated Nanoscience Lab, Department of Electrical and Information Engineering, and [§]Integrated Nanoscience Lab, Department of Material Science and Engineering, Harbin Institute of Technology, Shenzhen, 518055, China

Supporting Information

ABSTRACT: Very recently, perovskite based microdisk lasers have attracted considerable research attention. However, most of the researches are focused on the lasing spectra in bottom-up synthesized microdisks with regular shapes. The directionality, which is also essential for practical applications, has not been explored. Here we demonstrate unidirectional lasing emissions from perovskite microdisks for the first time. We synthesized the rectangle-shaped microdisks connected with straight waveguides and studied the lasing characteristics, where unidirectional emissions along the waveguides have been observed. Numerical calculations reveal that the unidirectional emissions are formed by the breaking of total internal reflections at the joints between waveguides and microdisks. Since waveguides are compatible with other photonic elements, we believe that our finding will be essential for the applications of perovskite microdisks in integrated photonic circuits and networks.

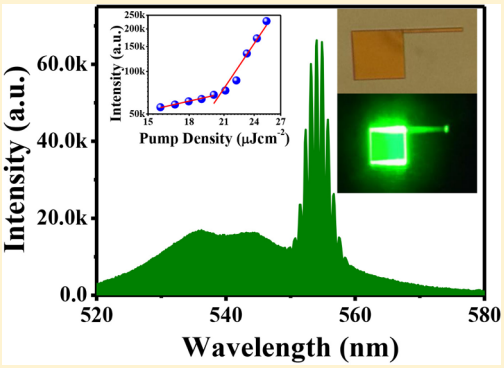

KEYWORDS: *perovskite microdisks, waveguide connected microdisks, unidirectional laser emissions, synthesis design*

Solution-processed perovskites have been intensively studied in the past few years.[1−14] This is mainly because of their potential applications in low-cost and high-efficiency solar cells.[1−6] In 2015, the light conversion coefficient of perovskites has been significantly improved to ∼20.1%.[7] Very recently, due to the relatively long carrier diffusion length and low trap-state density, perovskites have also started to show bright futures in optoelectronic devices.[8−10] Some perovskites such as $CH_3NH_3PbBr_3$ and $CH_3NH_3PbCl_3$ can emit light efficiently at green and blue wavelength ranges,[11] where conventional semiconductors (e.g., GaN) based microdisks face severe challenges in high quality fabrication.[15] Different from those kinds of top-down fabricated devices that have relatively rough boundaries, the bottom-up synthesized perovskites are usually single crystalline,[12] and the cavity boundaries can be naturally smooth. Thus, the conventional limitation of GaN devices can be easily resolved by the chemically grown organometallic halide perovskites. In past few years, lasing actions have been successfully observed in a number of micro- and nanosized devices, such as square microdisk,[12] rectangular microdisk, and triangular microdisks.[13] Up to now, great successes have been achieved in the observations of lasing actions in perovskite devices.[8−14,16,17] However, the directionality of perovskite microdisk laser, which is one of the key characteristics for practical applications, has been rarely studied.

Polygon-shaped microdisks usually have directional output.[18,19] Soon after the observation of laser emission from single crystalline device,[20] the mechanisms for the directional emissions of high quality (Q) resonances have been revealed.[17−22] Basically, the sharp corners of polygon play essential roles in light extraction. The evanescent waves can reach the corners and thus be scattered to far field. Meanwhile, slight deviation from stable orbits will finally leaks at the corners. These two mechanisms are well-known boundary wave leakage and pseudointegrable leakage, respectively.[18,19,22] However, as polygon microcavities have multiple corners, their far field patterns usually consist of multiple directional emissions. Even the Fabry−Perot (F−P) lasers produce two directional output beams.[17] These multiple emissions, associated with the large divergences in both in-plane and vertical directions, make microlaser emissions hard to be efficiently collected and utilized in practical applications. To overcome such limitations, waveguide connected microdisks (WCM) have been proposed and experimentally demonstrated.[23] Because the total internal reflections at the joints are broken, the directional emissions are mostly determined by the external waveguide instead of the corners. Meanwhile, as the external waveguide is independent of the resonant modes, the emissions along the waveguide direction can be easily collected without changing the internal resonant properties. Consequently, unidirectional emission along the waveguide has been widely studied in a number of laser systems, for example, triangular microdisk,[24] square microdisk,[23] hexagonal micro-

Received: March 26, 2016
Published: May 20, 2016

ACS Publications © 2016 American Chemical Society

DOI: 10.1021/acsphotonics.6b00209
ACS Photonics 2016, 3, 1125−1130

disk,[25] and quadruple microdisk.[26] However, due to their unique shapes, the WCMs are mostly fabricated by the top-down processes.[23−26] The bottom-up synthesized WCMs, which can be potentially used in blue and green lasers, have rarely been studied. In this research, we demonstrate the unidirectional emission from bottom-up synthesized single-crystalline perovskite microdisk. We show that WCMs can be chemically synthesized by a simple one-step solution-processed precipitation method. And thus the unidirectional emissions have been observed at the end of waveguides.

Following the previous studies,[27] it is easy to know that the synthesized rectangular microdisks have multiple directional emissions. Considering the fact that both perovskite microdisks and microwires have rectangular cavity shapes, we think it is possible to synthesize the waveguide connected microdisks and thus to improve the directionality. We first diluted the initial $CH_3NH_3Br{\cdot}PbBr_2$ solution to 0.05 M[17] and synthesized the $CH_3NH_3PbBr_3$ perovskite as above. Interestingly, the number of microwires increased significantly (Figure S1a−c). From the X-ray diffraction and selected area electron diffraction measurement, we knew that the microdisks and microwires were single crystallines (Figure S1d−f). Thus, we hypothesize that the microdisks with microwires can be directly grown. To test our conjecture, we changed the recipes and found that waveguide connected microdisk could be synthesized. Several parameters in the synthesis process have been considered. The high-quality perovskites microdisks were usually formed on hydrophobic substrate. Once the surface was changed to be hydrophilic, only huge blocks were obtained at the edges of substrate (Figure S3). Most importantly, the volumes of dropped solution and dichloromethane (DCM) must be strictly controlled to achieve the formation of waveguide connected microdisks. The number of waveguide connected microplates quickly reduces when the volumes of two solutions are changed (Figures S2 and S4).The typical perovskite microdisks are synthesized with the solution processed method.[12] Equal volumes of solutions of CH_3NH_3Br (0.2 M) and $PbBr_2$ (0.2 M) in DMF (*N*,*N*-dimethylformamide) were mixed, yielding stock solution-1 of $CH_3NH_3Br{\cdot}PbBr_2$ (0.1 M). Then solution-1 was dip-casted onto glass substrate. The glass substrate was placed onto a Teflon stage in a beaker containing DCM leveled below the Teflon stage. Then the dispersion of DCM vapor into $CH_3NH_3Br{\cdot}PbBr_2$ solution induced the nucleation and subsequent growth of perovskites. Figure 1a shows the typical scanning electron microscope (SEM) images of the synthesized perovskites. We can see that the synthesized perovskites are dominated by the rectangle-shaped microdisks. The lengths of such rectangular microdisks fall in a range from a few microns to tens of microns. The thicknesses of perovskite microdisks are around several hundred nanometers to several microns.

In this research, the synthesis conditions for waveguide connected microdisks have been optimized. Basically, 15 μL diluted solution-1 (0.05 M) was drop-coated onto an ITO substrate, whose hydrophobicity was improved by scribing the surface of ITO glass with a polyethylene film. The size of ITO glass is 14 × 14 mm^2. Then the substrate was also placed on a Teflon stage and sealed within a 250 mL beaker, where 75 mL DCM was added. After 24 h, perovskite micro- and nanostructures can be synthesized on ITO glass substrate. Figure 1b shows the SEM image of the synthesized perovskites. Within the measured area, we can clearly see thousands of nanowires and microwires that are covered by microblocks or microdisks. The sizes of microdisks also vary between a few

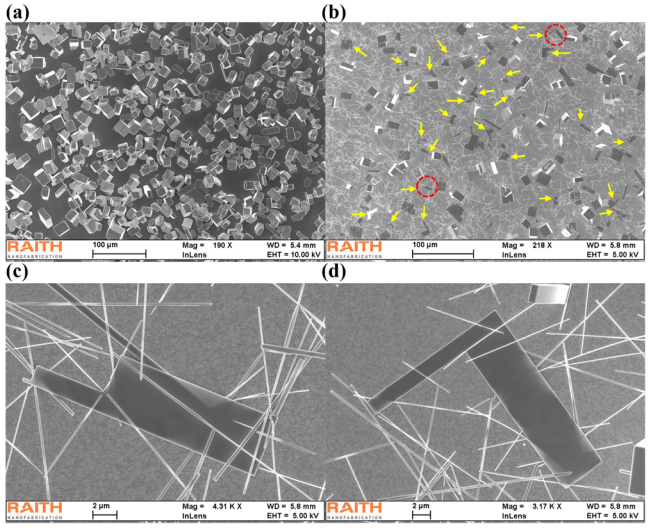

Figure 1. Top-view SEM images of synthesized perovskites with typical process (a) and with modified process (b). The yellow arrows in (b) mark the irregular microdisks that are directly connected with straight waveguides. (c, d) High-resolution SEM images of the waveguide connected microdisks marked in red dashed circle.

microns to tens of microns, too. But these microdisks show clearly different shapes from those in Figure 1a. More than 17% of the microdisks, which are marked by yellow arrows, have at least one straight waveguide directly connected onto their edges. Figure 1c,d shows the enlarged SEM images of these plates. We can see that the lengths of rectangular microdisks are usually around 5−30 μm and the widths of the waveguides are 0.5−4 μm. Distinct from the previous reports,[12] waveguide connected microdisks can be synthesized with nice reproducibility and repeatability following our proposed synthesis method (see Figure S6). $CH_3NH_3PbBr_3$ perovskite naturally crystallize into a cubic shape originating from the cubic phase structure. By finely controlling the synthesis conditions, such as the concentration and volume of the solution, the volume of dichloromehthane (DCM), hydrophobicity of sample surface, and the synthesis time, microwires and microplates could be synthesized simultaneously. Moreover, microwires typically have an overwhelmingly larger population than that of microplates. During the growth process, when microplate contacts microwire, as synthesis time goes by, a complex joint structure, waveguide connected microdisk (WCM) will come into being. The key to successful synthesis of the WCM is the simultaneous synthesis of microwire and microplate and the contact between them.

The as-grown waveguide connected microdisks are very similar to the top-down fabricated WCMs. As the total internal reflection at the joint position has been broken, we thus can expect the directional output along the straight waveguide. We selected one synthesized WCM (see the top-view SEM image in Figure 2a) and carried out the lasing experiment. The length and width of perovskite microdisk are 33.11 and 31.71 μm. And the length and width of straight waveguide are 39.43 and 2 μm, respectively. The thickness, which was recorded by the atomic force microscope (AFM), is 310 nm.

The lasing results are summarized in Figure 2. At a low pump density (P = 15.85 $\mu J\ cm^{-2}$), the emission spectrum was a broad peak of spontaneous emission (see Figure 2b). The full width at half-maximum (fwhm) was about 28 nm. With the increase of pump power, periodically sharp laser peaks gradually

DOI: 10.1021/acsphotonics.6b00209
ACS Photonics 2016, 3, 1125−1130

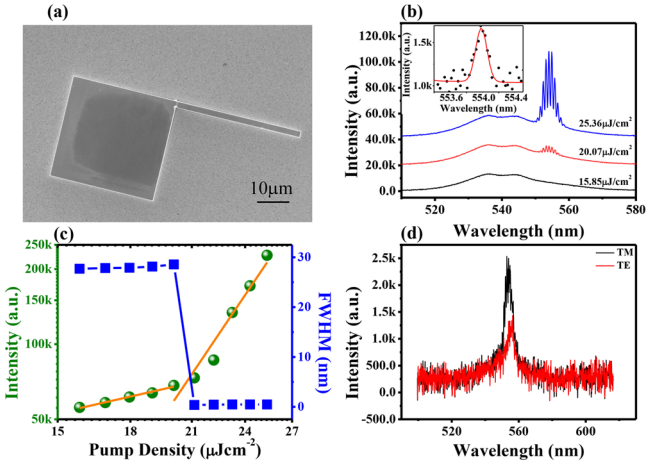

Figure 2. Top-view SEM image (a) of the WCM. The length and width of rectangle microplate are 33.11 and 31.71 μm, respectively. The width of waveguide is 2 μm, and the thickness of the WCM is 310 nm. (b) Emission spectra from WCM at different pump density. The spectra are vertically offset for clear view. Inset: the fitted fwhm of laser peak around the threshold. (c) Output intensity (green dots) and fwhm (blue squares) as a function of pump density. (d) Lasing polarization spectra of the WCM.

emerged in the laser spectrum (see Figure 2b). The mode spacing of the periodic modes is 0.86 nm. And the FWHMs dramatically transited to ~0.38 nm at P = 21 μJ cm^{-2}, which is more than an order of magnitude smaller than the spontaneous emission and gives a Q factor around 1460 (see the inset in Figure 2b). Figure 2c summarizes integrated intensity and fwhm as a function of pump density. When the pump density was low, the output intensity increased slowly and the slope in log−log plot is around 0.84, illustrating a simple spontaneous emission process. Once the pump density was above 21 μJ cm^{-2}, the output intensity increased dramatically and the slope was enhanced to more than 5.5. Such a dramatic transition from sublinear behavior to superlinear behavior clearly demonstrates the threshold behavior at 21 μJ cm^{-2}. Meanwhile, the fwhm dropped to 0.38 nm quickly at P = 21 μJ cm^{-2} and then slightly increased to around 0.47 nm at higher pumping density. This is caused by the band filling effect at higher pumping power.[12,13,17] Figure 2d shows lasing polarization of WCM with a polarizer switching from parallel (TE) to perpendicular (TM) to the WCM plane. Thus, we know that the lasing actions inside WCM are dominated by transverse magnetic (TM) polarization.

Compared with the confirmation of lasing actions, it is also interesting to explore the directional output of the synthesized WCM. Here we measured the near-field microscope image to determine the directionality (the reason will be discussed below). Figure 3a shows the recorded fluorescence microscope image, where the red dashed line corresponds to the pump laser spot. Similar to previous reports, the edges of microdisk became very bright once the pump density was above threshold. Interestingly, a clear bright spot can also be observed at the end of the unpumped straight waveguide in Figure 3a, even though emission light was absorbed along the straight waveguide. Considering the absorption loss and diffraction loss at the waveguide-microplate joint position (see Figure S11), the possibility of F−P lasers along the waveguide can be excluded. In this sense, here the bright spot should relate to the lasing emissions from rectangular microdisk. Following the previous

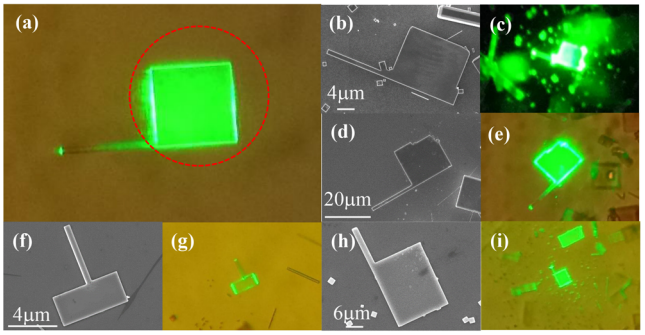

Figure 3. (a) Fluorescence microscope image of WCM above lasing threshold. Here the pump density is 31.64 μJ cm^{-2} and the pump area is marked with a red dashed circle. A bright spot can be observed at the end of the waveguide even though the waveguide has not been pumped. (b, d, f, h) Top-view SEM images of different synthesized perovskite WCMs. (c, e, g, i) Fluorescence microscope images of different WCMs. Clear bright spots can be observed at the ends of straight waveguides. Here the pump densities are all above lasing threshold.

research and the broken total internal reflection at the corner, we thus can expect that the leakages along the waveguide dominate the total emissions.

Importantly, we find that the bright spots at the end of the waveguide of WCM are quite generic in our synthesized samples. It has been observed in almost all the WCMs. Figure 3b,d,f,h shows the top-view SEM images of several other WCMs. While their sizes vary between a few microns and tens of microns, and the widths of waveguides change from a few hundred nanometers to a few microns, similar to Figure 3a, bright spots can be found at the ends of the connected waveguides in their corresponding fluorescence microscope images (see Figure 3c,e,g,i). This clearly demonstrates the emission along the waveguide is quite robust in our synthesized perovskite WCMs, no matter where the straight waveguides are connected.

After the observation of lasing actions and fluorescence microscope images, it is also interesting to explore the mechanism behind the formation of such lasing modes and corresponding directional emissions. Here we take the sample in Figure 2 as an example. As the height of perovskite WCM is orders of magnitude smaller than the in-plane size, the WCM can be simply simulated by employing a 2D simulation model (2D eigenfrequency model, Comsol Multiphysics 3.5a) via effective refractive index (n_{eff} = 2.45, which is calculated from the fundamental mode based on 2D mode analysis model). Following the simple ray optics, a number of orbit families can be formed within the rectangular microdisk. The most well-known one is the four-bounce diamond orbit family (Figure S10), which has the smallest bouncing angle around 43.75°. Another one is the double-diamond orbit family (see Figure 4a) that has the smallest bouncing angle around 27.57°. Due to the relatively large effective refractive index (corresponding to a critical angle θ = 24.1°), the light along the second orbit family can still be well trapped by total internal reflection. Following the mode spacings in Figure 2b and the cavity length along the orbit family, the effective refractive index in experiment can thus be estimated with the equation $n_{eff} = \lambda^2/\Delta\lambda L$. The length of diamond orbit is around 91.38 μm, giving an effective refractive index n_{eff} = 3.92. This value is much larger than the typical refractive index of $CH_3NH_3PbBr_3$ perovskites. One may quickly consider the group index, which is usually written as n_g

DOI: 10.1021/acsphotonics.6b00209
ACS Photonics 2016, 3, 1125−1130

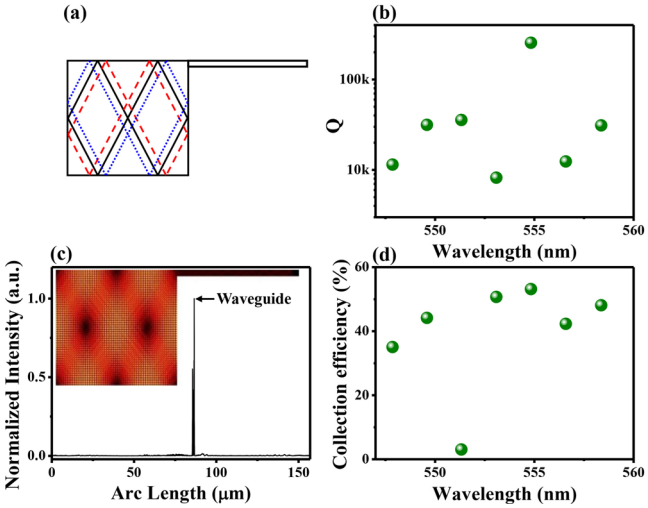

Figure 4. (a) Schematic diagram of double-diamond orbit family. (b) Calculated Q factors of modes along double-diamond orbit family within the lasing frequency range. (c) Calculated far field pattern of the highest-Q mode in (b). Inset shows the corresponding field distribution. (d) Calculated collection efficiency of modes along double-diamond orbit family within the lasing frequency range.

$= n - \lambda dn/d\lambda$. However, from the measured refractive index, the group index is still far below the estimated value (Figure S9). Moreover, we have also studied the lasing spectra of one microwire from the same substrate. The mode spacing gives an estimated refractive index around 5.2 (Figure S9). In principle, the group index of single crystal will not change so dramatically from the same material. Consequently, we should pay attention to the other long-lived resonances. The length of double-diamond orbit is 142.59 μm, which corresponds to an effective refractive index $n_{eff} = 2.51$. This effective refractive index is very close to the estimated n_{eff}. The slight difference should be caused by group index.[12,21,28] Therefore, the lasing modes in Figure 2b should be formed along the double-diamond orbit family.

To confirm above analysis, we then numerically studied the resonant properties of perovskite WCM with a finite element method based commercial software (COMSOL Multiphysics).[29] Due to the openness of the cavity, eigenfrequencies with complex values (ω) are obtained and the cavity quality (Q) factor can be expressed as $Q = \mathrm{Re}(\omega)/|2\mathrm{Im}(\omega)|$. Restricted from the computer hardware, the size of WCM in simulation was halved and, thus, the corresponding mode spacing will be doubled. Figure 4b shows the calculated Q factors of modes along double-diamond orbit family within the lasing frequency range. We can see that the mode spacing is about 1.75 nm, which is more than twice of experimentally measured mode spacing. This is consistent with our initial expectation (the mode spacing is doubled because the cavity size is halved). And their Q factors of double-diamond resonances are usually much larger than 10^4, as shown in Figure 4b. Some mode with external mode coupling can even have a Q factor as high as 2×10^5.[29] This kind of high Q resonance is formed by the field distributions. While the total internal reflection at the joint position is broken, as shown in the inset of Figure 4c, the main field distribution is localized away from the corners and the waveguide. Such field distributions can be understood as follows: In general, the orbit family can be unfolded to a straight waveguide and the corresponding resonances can be considered as waveguide modes.[30,31] Thus, most of the energy will be confined away from the edge of unfolded waveguide where the corners and the external waveguide exist.

Considering the propagating modes in unfolded waveguide, there are still some tiny field distributions at the edges. Therefore, connecting a straight waveguide around one corner can break the total internal reflection and efficiently conduct the leakages from microdisk along the waveguide. Even though the field distribution is weak at the corner, it is still much larger than the evanescent waves out of the corners. In this sense, the direct transmission leakage to the external waveguide will be much larger than the conventional boundary wave leakage[18] and thus dominate the far field emission. Figure 4c shows the calculated far field emission of the mode at 554.83 nm. Similar to the analysis, we can see that the emission along the waveguide is much larger than the other directions in free space. The collection efficiency of energy inside the waveguide (U) is more than 53% of total emissions. This means that most of the emission will be collected by the external waveguide of WCM. Figure 4d summarizes the collection efficiencies of all the resonant modes in Figure 4b. While the exact value varies a little bit, all the resonances except for one mode at 551.33 nm, have relatively large U factors. The mode at 551.33 nm should be caused by the interaction with nearby resonances.[26] Then all the lasing modes should have similar far field emissions along the waveguide. Therefore, the far field pattern of perovskite based WCM can be simply determined by the fluorescence microscope image (see Figure 3 for examples).

It must be noted that the fluorescence microscope images can be a clue but far from enough to confirm the unidirectional emissions along the waveguide. To directly confirm the

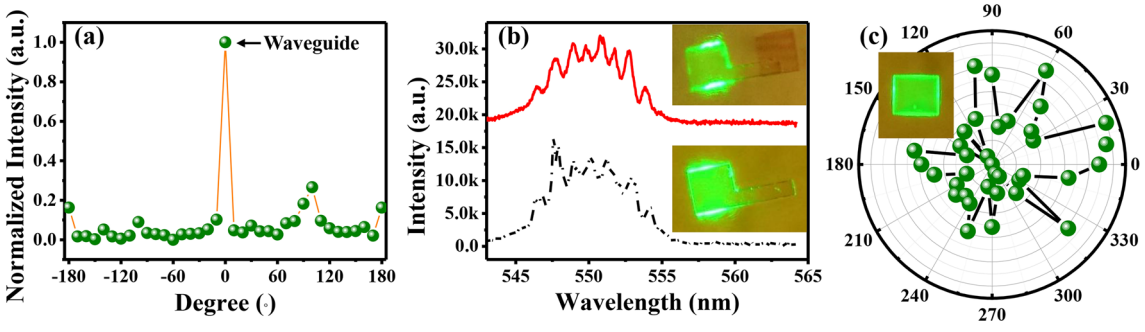

Figure 5. (a) Output intensity measured from another WCM, where 0° corresponds to output waveguide direction. (b) Lasing spectra from the WCM. Insets are corresponding fluorescence images with and without a perovskite block. (c) Output intensity measured from a rectangular microdisk without additional waveguide. The inset is the corresponding fluorescent microscope image.

DOI: 10.1021/acsphotonics.6b00209
ACS Photonics 2016, 3, 1125−1130

numerical simulation, we have carefully measured the in-plane emissions from the microdisk. Here we collect the emissions from microdisk with a tapered fiber very close to the microdisk. During the measurement, the lasing emission was collected in a circular orbit where the center was located at the center of microdisk and the radius was the distance from the center of square microdisk to the end of waveguide. As the previous samples were destroyed in experiment, here we synthesized the WCM again and measured the emissions. The synthesized WCM is shown as bottom inset in Figure 5b. And the corresponding output intensity is shown in Figure 5a. We can see that the emission intensity along the waveguide (0°) is much larger than the other directions in free space. This result is consistent with the numerical simulation and clearly shows that the unidirectional emission along the waveguide. To further confirm the directionality of WCM, a control measurement on pure microdisk has been conducted in the same measurement way and the result is shown in Figure 5c. Instead of unidirectional emission, four directional output beams can be readily seen along the sides of of rectangular microdisk.

To further exclude the possibility of F−P modes, a perovskite block was moved to the output end of waveguide via micromanipulation, as shown in the upper inset of Figure 5b. In principle, the refractive index of the block is the same as the waveguide and thus can induce significant loss to the F−P modes along the waveguide. The block can suppress the F−P modes well.[32] Thus, we can simply know that the lasing modes will be strongly destroyed if they are formed along the F−P modes. Here the experimental results show a quite different phenomenon. As shown in Figure 5b, the peak number and peak positions of the laser spectra with and without block are almost the same. Therefore, we can know that the lasing modes in our cavities should not follow the F−P resonances.

In summary, we have experimentally synthesized the waveguide connected perovskite microdisks via simple solution-processed precipitation method. By directly connecting a waveguide to a rectangular microdisk, the total internal reflection at the joint is broken and unidirectional lasing emission from perovskite microdisk has been observed for the first time. Unlike the conventional polygon shaped microdisks that have multiple directional outputs in free space, here the unidirectional output is well confined within the waveguide. Considering the compatibility of waveguide and other optical elements, such kind of perovskite lasers with unidirectional emissions have two intrinsic advantages and can be potentially applied in integrated optical circuits and optical interconnect. (1) It can generate unidirectional emission, which is essential for light collection and coupling. (2) The waveguide is mainly used to collect and conduct the emission light which is independent to the main resonances. We believe this research will be important for the development and applications of perovskite microlasers.

■ ASSOCIATED CONTENT

Supporting Information

The Supporting Information is available free of charge on the ACS Publications website at DOI: 10.1021/acsphotonics.6b00209.

Synthesis condition optimization, optical experiment setup, lasing emissions from another waveguide connected microdisk, group index, and additional numerical simulation (PDF).

■ AUTHOR INFORMATION

Corresponding Author

*E-mail: qinghai.song@hitsz.edu.cn.

Author Contributions

‡These authors contributed equally.

Notes

The authors declare no competing financial interest.

■ ACKNOWLEDGMENTS

This work is supported by NSFC11204055, NSFC61222507, NSFC11374078, NCET-11-0809, Shenzhen Peacock plan under the No. KQCX20130627094615410, and Shenzhen Fundamental research projects under the No. JCYJ20140417172417096.

■ REFERENCES

(1) Shi, D.; Adinolfi, V.; Comin, R.; Yuan, M. J.; Alarousu, E.; Buin, A.; Chen, Y.; Hoogland, S.; Rothenberger, A.; Katsiev, K.; Losovyj, Y.; Zhang, X.; Dowben, P. A.; Mohammed, O. F.; Sargent, E. H.; Bakr, O. M. Low trap-state density and long carrier diffusion in organolead trihalide perovskite single crystals. *Science* **2015**, *347*, 519−522.

(2) Ning, Z. J.; Gong, X. W.; Comin, R.; Walters, G.; Fan, F. J.; Voznyy, O.; Yassitepe, E.; Buin, A.; Hoogland, S.; Sargent, E. H. Quantum-dot-in-perovskite solids. *Nature* **2015**, *523*, 324−328.

(3) Liu, M.; Johnson, M. B.; Snaith, H. J. Efficient planar heterojunction perovskite solar cells by vapour deposition. *Nature* **2013**, *501*, 395−398.

(4) Heo, J. H.; Im, S. H.; Noh, J. H.; Mandal, T. N.; Lim, C. S.; Chang, J. A.; Lee, Y. H.; Kim, H. J.; Sarkar, A.; Nazeeruddin, M. K.; Grätzel, M.; Seok, S. I. Efficient inorganic-organic hybrid heterojunction solar cells containing perovskite compound and polymeric hole conductors. *Nat. Photonics* **2013**, *7*, 486−491.

(5) Green, M. A.; Ho-Baillie, A.; Snaith, H. J. The emergence of perovskite solar cells[J]. Nature Photonics. *Nat. Photonics* **2014**, *8*, 506−514.

(6) Xing, G.; Mathews, N.; Sun, S.; Lim, S. S.; Grätzel, M.; Mhaisalkar, S.; Sum, T. C. Long-range balanced electron-and hole-transport lengths in organic-inorganic $CH_3NH_3PbI_3$. *Science* **2013**, *342*, 344−347.

(7) Yang, W. S.; Noh, J. H.; Jeon, N. J.; Kim, Y. C.; Ryu, S.; Seo, J.; Seok, S. I. High-performance photovoltaic perovskite layers fabricated through intramolecular exchange. *Science* **2015**, *348*, 1234−1237.

(8) Xing, G.; Mathews, N.; Lim, S. S.; Yantara, N.; Liu, X.; Sabba, D.; Grätzel, M.; Mhaisalkar, S.; Sum, T. C. Low-temperature solution-processed wavelength-tunable perovskites for lasing. *Nat. Mater.* **2014**, *13*, 476−480.

(9) Ha, S. T.; Liu, X.; Zhang, Q.; Giovanni, D.; Sum, T. C.; Xiong, Q. Synthesis of Organic−Inorganic Lead Halide Perovskite Nanoplatelets: Towards High-Performance Perovskite Solar Cells and Optoelectronic Devices. *Adv. Opt. Mater.* **2014**, *2*, 838−844.

(10) Schmidt, L. C.; Petegas, A.; Carrero, S. G.; Malinkiewicz, O.; Agouram, S.; Espallargas, G. M.; Bolink, H. J.; Galian, R. E.; Prieto, J. P. Nontemplate synthesis of $CH_3NH_3PbBr_3$ perovskite nanoparticles. *J. Am. Chem. Soc.* **2014**, *136*, 850−853.

(11) Xing, J.; Liu, X. F.; Zhang, Q.; Ha, S. T.; Yuan, Y. W.; Shen, C.; Sum, T. C.; Xiong, Q. Vapor phase synthesis of organometal halide perovskite nanowires for tunable room-temperature nanolasers. *Nano Lett.* **2015**, *15*, 4571−4577.

(12) Liao, Q.; Hu, K.; Zhang, H. H.; Wang, X. D.; Yao, J. N.; Fu, H. B. Perovskite Microdisk Microlasers Self-Assembled from Solution[J]. Advanced Materials. *Adv. Mater.* **2015**, *27*, 3405−3410.

DOI: 10.1021/acsphotonics.6b00209
ACS Photonics 2016, 3, 1125−1130

(13) Zhang, Q.; Ha, S. T.; Liu, X. F.; Sum, T. C.; Xiong, Q. H. Room-temperature near-infrared high-Q perovskite whispering-gallery planar nanolasers. *Nano Lett.* **2014**, *14*, 5995−6001.
(14) Zhu, H. M.; Fu, Y. P.; Meng, F.; Wu, X. X.; Gong, Z. Z.; Ding, Q.; Gustafsson, M. V.; Trinh, M. T.; Jin, S.; Zhu, X. Y. Lead halide perovskite nanowire lasers with low lasing thresholds and high quality factors. *Nat. Mater.* **2015**, *14*, 636−642.
(15) Tamboli, A. C.; Haberer, E. D.; Sharma, R.; Lee, K. H.; Nakamura, S.; Hu, E. L. Room-temperature continuous-wave lasing in GaN/InGaN microdisks. *Nat. Photonics* **2007**, *1*, 61−64.
(16) Yakunin, S.; Protesescu, L.; Krieg, F.; Bodnarchuk, M. I.; Nedelcu, G.; Humer, M.; Luca, G. D.; Fiebig, M.; Heiss, W.; Kovalenko, M. V. Low-threshold amplified spontaneous emission and lasing from colloidal nanocrystals of caesium lead halide perovskites. *Nat. Commun.* **2015**, *6*, 8056.
(17) Gu, Z. Y.; Wang, K. Y.; Sun, W. Z.; Li, J. K.; Liu, S.; Song, Q. H.; Xiao, S. M. Two-Photon Pumped CH3NH3PbBr3 Perovskite Microwire Lasers. *Adv. Opt. Mater.* **2016**, *4*, 472−479.
(18) Braun, I.; Ihlein, G.; Laeri, F.; Nöckel, J. U.; Ekloff, G. S.; Schüth, F.; Vietze, U.; Weiss, Ö.; Wöhrle, D. Hexagonal microlasers based on organic dyes in nanoporous crystals. *Appl. Phys. B: Lasers Opt.* **2000**, *70*, 335−343.
(19) Wiersig, J. Hexagonal dielectric resonators and microcrystal lasers. *Phys. Rev. A: At., Mol., Opt. Phys.* **2003**, *67*, 023807.
(20) Odoulov, S. G.; Goulkov, M. Y.; Shinkarenko, O. A. Threshold behavior in formation of optical hexagons and first order optical phase transition. *Phys. Rev. Lett.* **1999**, *83*, 3637.
(21) Lebental, M.; Djellali, N.; Arnaud, C.; Lauret, J.-S.; Zyss, J.; Dubertrand, R.; Schmit, C.; Bogomolny, E. Inferring periodic orbits from spectra of simply shaped microlasers. *Phys. Rev. A: At., Mol., Opt. Phys.* **2007**, *76*, 023830.
(22) Song, Q. H.; Ge, L.; Wiersig, J.; Cao, H. Formation of long-lived resonances in hexagonal cavities by strong coupling of superscar modes. *Phys. Rev. A: At., Mol., Opt. Phys.* **2013**, *88*, 023834.
(23) Huang, Y. Z.; Che, K. J.; Yang, Y.-D.; Wang, S. J.; Du, Y.; Fan, Z. C. Directional emission InP/GaInAsP square-resonator microlasers. *Opt. Lett.* **2008**, *33*, 2170−2172.
(24) Huang, Y. Z.; Hu, Y. H.; Chen, Q.; Wang, S. J.; Du, Y.; Fan, Z. C. Room-temperature continuous-wave electrically injected InP−GaInAsP equilateral-triangle-resonator lasers. *IEEE Photonics Technol. Lett.* **2007**, *19*, 963−965.
(25) Lin, J. D.; Huang, Y.-Z.; Yang, Y. D.; Yao, Q. F.; Lv, X. M.; Xiao, J. L.; Du, Y. Single transverse whispering-gallery mode AlGaInAs/InP hexagonal resonator microlasers. *IEEE Photonics J.* **2011**, *3*, 756−764.
(26) Song, Q. H.; Ge, L.; Redding, B.; Cao, H. Channeling chaotic rays into waveguides for efficient collection of microcavity emission. *Phys. Rev. Lett.* **2012**, *108*, 243902.
(27) Ling, T.; Liu, L. Y.; Song, Q. H.; Xu, L.; Wang, W. C. Intense directional lasing from a deformed square-shaped organic-inorganic hybrid glass microring cavity. *Opt. Lett.* **2003**, *28*, 1784−1786.
(28) Long, H.; Huang, Y. Z.; Yang, Y. D.; Zou, L. X.; Xiao, J. L.; Xiao, Z. X. Mode and modulation characteristics for microsquare lasers with a vertex output waveguide. *Sci. China: Phys., Mech. Astron.* **2015**, *58*, 114205.
(29) Wang, K. Y.; Gu, Z. Y.; Sun, W. Z.; Li, J. K.; Xiao, S. M.; Song, Q. H. Quasi-guiding Modes in Microfibers on a High Refractive Index Substrate. *ACS Photonics* **2015**, *2*, 1278−1283.
(30) Bogomolny, E.; Schmit, C. Structure of wave functions of pseudointegrable billiards. *Phys. Rev. Lett.* **2004**, *92*, 244102.
(31) Bogomolny, E.; Dietz, B.; Friedrich, T.; Miski-Oglu, M.; Richter, A.; Schäfer, F.; Schmit, C. First experimental observation of superscars in a pseudointegrable barrier billiard. *Phys. Rev. Lett.* **2006**, *97*, 254102.
(32) Wang, K. Y.; Gu, Z. Y.; Liu, S.; Li, J. K.; Xiao, S. M.; Song, Q. H. Formation of single-mode laser in transverse plane of perovskite microwire via micromanipulation. *Opt. Lett.* **2016**, *41*, 555−558.

DOI: 10.1021/acsphotonics.6b00209
ACS Photonics 2016, 3, 1125−1130